

# Microstructures and mechanical properties of Mg–Zn–Zr–Dy wrought magnesium alloys

Z H HUANG<sup>†,‡,\*</sup>, W J QI<sup>†</sup>, K H ZHENG<sup>†</sup>, X M ZHANG<sup>‡</sup>, M LIU<sup>†</sup>, Z M YU<sup>‡</sup> and J XU<sup>†</sup>

<sup>†</sup>Guangzhou Research Institute of Non-ferrous Metals, Guangzhou 510650, P.R. China

<sup>‡</sup>School of Materials Science and Engineering, Central South University, Changsha 410083, P.R. China

MS received 19 February 2012; revised 6 June 2012

**Abstract.** Microstructures and phase compositions of as-cast and extruded ZK60–*x*Dy (*x* = 0–5) alloys were analysed by optical microscope, scanning electron microscope, X-ray diffraction and differential scanning calorimetry. Meanwhile, the tensile mechanical property was tested. With increasing Dy content, Mg–Zn–Dy new phase increases gradually, while MgZn<sub>2</sub> phase decreases gradually to disappear. As-cast microstructure is refined gradually; meanwhile extruded one is refined further with decreasing average grain size to 1 μm for ZK60–4.32Dy alloy. Second phase, tending to distribute along grain boundary by continuous network in as-cast state, breaks and distributes dispersedly in extrusion state. As-cast tensile mechanical property remains almost unchanged at ambient temperature; however, extruded ones are enhanced significantly at ambient and elevated temperatures, respectively. Tensile strength at 298 and 473 K increases gradually from 355 and 120 MPa for ZK60 alloy to 395 and 171 MPa for ZK60–4.32Dy alloy, respectively. Extruded tensile fractures exhibit a typical character of ductile fracture.

**Keywords.** Wrought magnesium alloys; microstructure; mechanical property; extrusion.

## 1. Introduction

Magnesium alloys are one of the most important structural materials having high specific strength and used widely in automotive, communication, electronic and aerial industries (Polmear 1994). Wrought magnesium alloys exhibit higher strength, better ductility and comprehensive property, however, they still do relatively poor plasticity and corrosion resistance owing to the limit of hexagonal close packed crystal structure and low electrode potential for Mg, respectively (Chen 2005). Therefore, it is necessary to develop new wrought magnesium alloys with high performance by investigating the deformation mechanism. Rare-earth (RE) with unique atomic electron and chemical property can purify the alloy melt, ameliorate the microstructure, and enhance both the mechanical property and the corrosion resistance effectively. Researchers had studied the effects of Y (Luo *et al* 1995; Xu *et al* 2007), Ce (Xia *et al* 2005), Nd (Li *et al* 2007), Gd (He *et al* 2006), Yb (Yu *et al* 2008) and Ho (Li *et al* 2011) on the microstructure and mechanical property of widely used ZK60 wrought magnesium alloy extensively; however, the effect of Dy has been rarely studied yet. Strengthening mechanism has not been cleared entirely for magnesium alloys yet. As well as the grain size, the type, morphology, distribution and volume fraction of second phase can also

affect the mechanical property significantly (Li *et al* 2007). Therefore, the present paper is focused on studying the microstructures and tensile mechanical properties at ambient and elevated temperatures of as-cast and extruded ZK60–*x*Dy (*x* = 0–5) alloys in detail, and then discussing the role of second phase on the strengthening and deformation mechanisms.

## 2. Experimental

Chemical compositions of as-cast ZK60–*x*Dy alloys measured by inductively coupled plasma analyser (ICP, JY Ultima2) are listed in table 1. Alloy ingots were prepared by melting pure Mg, pure Zn and Mg–30 wt% Zr, Mg–30 wt% Dy master alloys in electric resistance furnace under the mixed atmosphere of N<sub>2</sub> and SF<sub>6</sub>. When the melt temperature of pure Mg reached 1003 K, pure Zn and two master alloys were added into the melt in turn. Then the melt was stirred twice within an hour to ensure the compositional homogeneity. After adding the refined agent (JDMJ) mainly consisting of 40–60 wt% MgCl<sub>2</sub>, 10–25 wt% KCl and 10–25 wt% NaCl, the melt was held at 1033 K for 30 min. When the temperature cooled to 988 K, the melt was poured into the wedge permanent mold with pre-heated temperature of 523 K and then as-cast samples were obtained. Cast rods could also be obtained by pouring the melt into the circular permanent mold with a diameter of 110 mm under the same technology. They were homogenized at 673 K for

\*Author for correspondence (zhhuang@live.cn)

8 h in the heat-treating furnace and then machined to a diameter of 100 mm. Extrusion rods were obtained by extruder with extrusion ratio,  $\lambda$ , extrusion temperature,  $T$  and extrusion speed,  $V$  of 40, 593 K and 1~2 m/min, respectively.

As-cast and extruded specimens were etched with 4 vol%  $\text{HNO}_3$  in ethanol and a solution of 1.5 g picric acid, 25 ml ethyl alcohol, 5 ml acetic acid plus 10 ml distilled water, respectively. Microstructural observation was carried out on optical microscope (OM, Leica DM IRM) and scanning electron microscope (SEM, JEOL JXA-8100) with energy dispersive spectroscopy (EDS, OXFORD 7412). Volume fraction,  $f$ , of second phase among as-cast SEM graph was calculated by the accessory analysis software of Leica

optical microscope. Tensile fractograph at ambient temperature was observed using SEM. Phase analysis was carried out on X-ray diffractometer (XRD, D/MAX-RC) with  $\text{CuK}\alpha$  radiation. Phase change during the heating process was characterized by isochronal heating in differential scanning calorimeter (DSC, Netzsch STA409) under flow of highly-purified Ar atmosphere at a rate of 20 K/min. Small standard plate and rod tensile specimens with gauge length of 25 mm and section of  $6 \times 3 \text{ mm}^2$  or diameter of 5 mm, respectively were machined for as-cast and extruded samples, respectively. Tensile test at a temperature range from 298 to 473 K was performed on material test machine (GP-TS2000) at a rate of 2 mm/min.

**Table 1.** Chemical composition of ZK60- $x$ Dy alloys (wt%).

	Zn	Zr	Dy	Mg
ZK60	5.83	0.66		Bal.
ZK60-0.31Dy	5.82	0.67	0.31	Bal.
ZK60-0.70Dy	5.81	0.62	0.70	Bal.
ZK60-1.15Dy	5.81	0.64	1.15	Bal.
ZK60-2.18Dy	5.82	0.59	2.18	Bal.
ZK60-3.18Dy	5.70	0.57	3.18	Bal.
ZK60-4.32Dy	5.69	0.56	4.32	Bal.

### 3. Results

#### 3.1 Microstructures and mechanical properties of as-cast ZK60- $x$ Dy alloys

Figures 1 and 2 show optical and SEM graphs of as-cast ZK60- $x$ Dy alloys, respectively. The change in the average grain size,  $\bar{d}$  and volume fraction,  $f$ , of second phase is shown in figure 3. As-cast ZK60 alloy exhibits coarse microstructure and few dispersed second phases. With

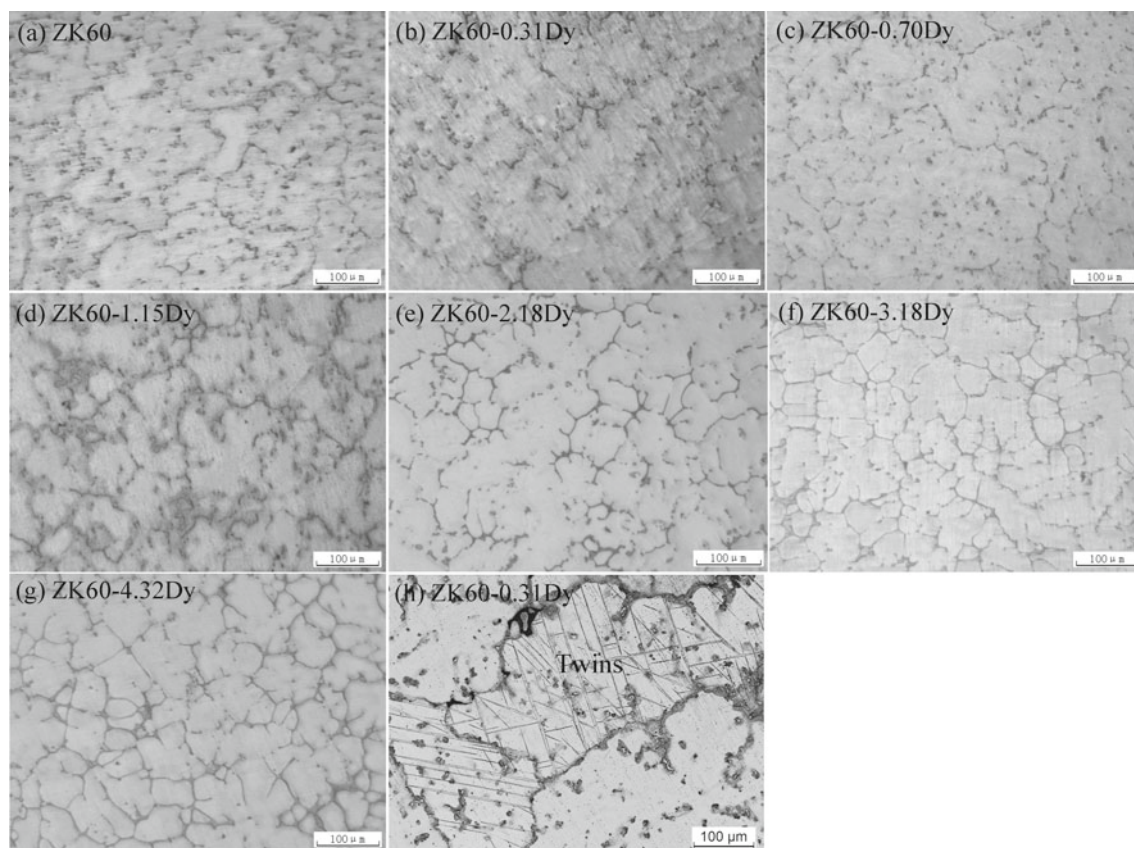


**Figure 1.** Optical graphs of as-cast ZK60- $x$ Dy alloys etched with 4 vol%  $\text{HNO}_3$  in ethanol (a–g) and a solution of picric acid (h), respectively.

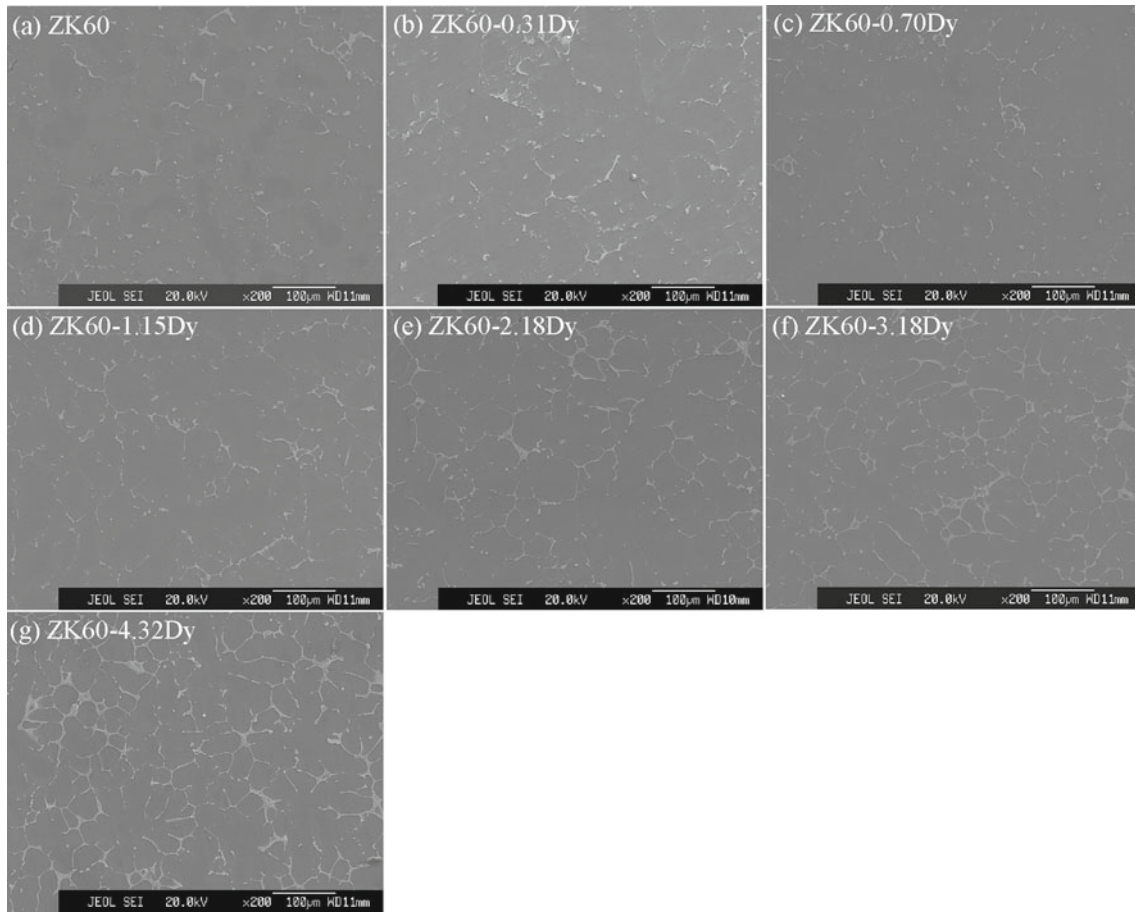


Figure 2. SEM graphs of as-cast ZK60– $x$ Dy alloys.

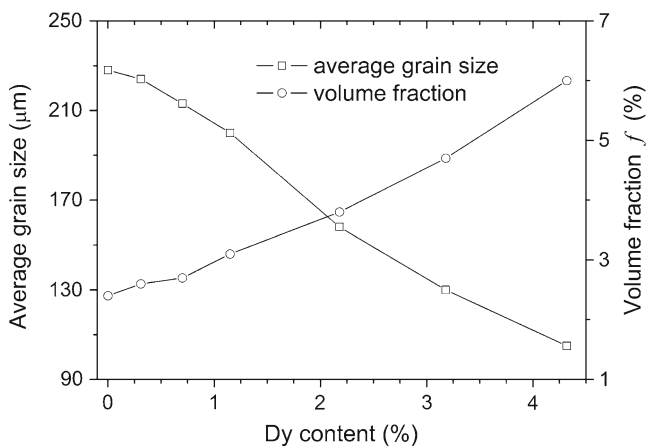


Figure 3. Average grain size and volume fraction,  $f$ , of second phase of as-cast ZK60– $x$ Dy alloys.

increasing Dy content, as-cast microstructure is refined gradually, where  $\bar{d}$  decreases gradually from 228  $\mu\text{m}$  for ZK60 alloy to 105  $\mu\text{m}$  for ZK60–4.32Dy alloy. Meanwhile, second phase increases gradually from  $f = 2.4\%$  to  $f = 6\%$  and tends to distribute along the grain boundary by

continuous network. In addition, dislocation can slip on a large scale within coarse grain and stress concentrates near grain boundary, which meet the requirement of forming twin nucleus. Thus, twins can be observed clearly within one grain or few adjacent grains among all as-cast microstructures etched with a solution of picric acid (see figure 1h).

Figure 4 shows EDS spectra of as-cast alloys and the results are listed in table 2. For as-cast ZK60 alloy, there exists two different Mg–Zn phases containing relatively low and high Zr contents, respectively while Mg–Zn–Dy new phase occurs and no Mg–Zn phase can be observed for as-cast ZK60–0.31Dy and ZK60–4.32Dy alloys. However, the atomic ratio in Mg–Zn phase is slightly different from that determined by following XRD patterns owing to the influence by adjacent  $\alpha$ -Mg matrix and that in Mg–Zn–Dy phase changes slightly with most of Dy content of about 5 at%. Majority of Zn element distributes along grain boundary to form  $\text{MgZn}_2$  phase for as-cast ZK60 alloy. Similar to Zn element, Dy element also distributes mainly along grain boundary to form Mg–Zn–Dy phase for as-cast ZK60–4.32Dy alloy (see figure 5).

In order to determine new phase owing to the addition of Dy, comparison between XRD spectra of as-cast ZK60 and ZK60–4.32Dy alloys was made (see figure 6a). XRD



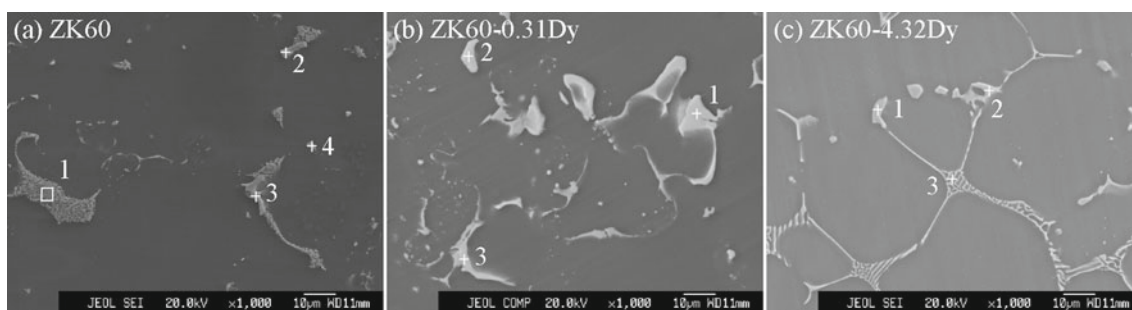


Figure 4. EDS spectra of as-cast ZK60- $x$ Dy alloys.

Table 2. EDS results of as-cast ZK60- $x$ Dy alloys (at%).

		Mg	Zn	Zr	Dy
ZK60	Spectrum 1	61.87	38.06	0.07	
	Spectrum 2	21.11	60.29	18.60	
	Spectrum 3	30.15	54.58	15.27	
	Spectrum 4	72.78	26.97	0.25	
ZK60-0.31Dy	Spectrum 1	42.26	52.67		5.07
	Spectrum 2	39.77	54.36		5.88
	Spectrum 3	39.88	55.02		5.10
ZK60-4.32Dy	Spectrum 1	50.13	43.48		6.39
	Spectrum 2	47.07	36.12		16.81
	Spectrum 3	75.30	16.88		7.83

spectrum of as-cast ZK60 alloy consists of the peaks of  $\alpha$ -Mg and  $\text{MgZn}_2$  phases, while the peak of  $\text{MgZn}_2$  phase disappears completely and that of an unknown phase, but not Mg-Dy binary phase, can be observed among the XRD spectrum of as-cast ZK60-4.32Dy alloy. Combined with the EDS results, the unknown phase is considered as Mg-Zn-Dy phase. This indicates that added Dy atoms combine with Mg and Zn atoms to form Mg-Zn-Dy new phase on priority.

Figure 6(b) shows the isochronal heating of DSC curves of as-cast alloys and peak temperatures,  $T_{\text{P1}}$ , of endothermic peaks are listed in table 3. For as-cast ZK60 alloy, there exists two distinct endothermic peaks with  $T_{\text{P1}}$  and  $T_{\text{P2}}$  of 618 and 902 K, which are close to the melting point,  $T_{\text{m}}$  (620 and 923 K) of  $\text{MgZn}_2$  phase and  $\alpha$ -Mg matrix, respectively. Thus, the two endothermic peaks should be corresponding to the melting of the two phases, respectively. For as-cast ZK60-0.31Dy alloy, the two endothermic peaks still exist with the significantly weak first one, and meanwhile a new one occurs at 735 K. For as-cast ZK60-4.32Dy alloy, the endothermic peak at about 620 K disappears completely, while another new one occurs at 828 K on the basis of retaining others. Although  $T_{\text{m}}$  of Mg-Zn-Dy phase cannot be looked up currently, the endothermic peaks at the temperature range from 731 to 828 K for the two Dy-containing alloys should be corresponding to the melting of the phase containing different

Dy contents. This indicates that Mg-Zn-Dy phase exhibits higher thermal stability than  $\text{MgZn}_2$  phase.

As-cast tensile mechanical property remains almost unchanged at ambient temperature with increasing Dy content (see figure 7a). Tensile strength,  $\sigma_{\text{b}}$  and yield strength,  $\sigma_{0.2}$ , change at the range of 215–225 MPa and 110–135 MPa, respectively. Meanwhile, elongation,  $\delta$ , is not lower than 7.0%, which may be related to the occurrence of twins among as-cast microstructure. All as-cast tensile fractures exhibit a complex mode of ductile and brittle fractures (see figure 8a–c). Dimples occupy the majority, while cleavage steps and river patterns are few for as-cast ZK60 alloy. Dimples decrease slightly with increasing Dy content, which is consistent with the slight decrease in the elongation.

### 3.2 Microstructures and mechanical properties of extruded ZK60- $x$ Dy alloys

ZK60, ZK60-0.31Dy and ZK60-4.32Dy alloys were chosen to study the effect of Dy content on the extruded microstructure and tensile mechanical property. Optical and SEM graphs in the extrusion direction are shown in figures 9 and 10, respectively. Compared with as-cast state, extruded microstructure is refined significantly owing to the dynamic recrystallization during the hot deformation process. For extruded ZK60 alloy, dynamic recrystallization grains (DRGs) change at a size ranging from 2 to 10  $\mu\text{m}$  with  $\bar{d}$  of 5  $\mu\text{m}$ . Meanwhile majority of  $\text{MgZn}_2$  phase dissolved through homogenization does not re-precipitate during the hot deformation process. With increasing Dy content, DRGs become unique and  $\bar{d}$  gradually decreases to 1  $\mu\text{m}$  for extruded ZK60-4.32Dy alloy. Meanwhile, second phase breaks and distributes dispersedly.

Compared with as-cast state, extruded tensile-mechanical property is enhanced significantly at ambient temperature (see figure 7b–d).  $\sigma_{\text{b}}$ ,  $\sigma_{0.2}$  and  $\delta$  can reach 355, 300 MPa and 19.5% for extruded ZK60 alloy, respectively. As the Dy content increases,  $\sigma_{\text{b}}$  and  $\sigma_{0.2}$  increase gradually to 395 and 355 MPa for extruded ZK60-4.32Dy alloy, respectively.  $\delta$  decreases gradually, but not lower than 12%. With increasing test temperature,  $\sigma_{\text{b}}$  and  $\sigma_{0.2}$  decrease gradually, while  $\delta$  increases gradually. For extruded ZK60 alloy,  $\sigma_{\text{b}}$

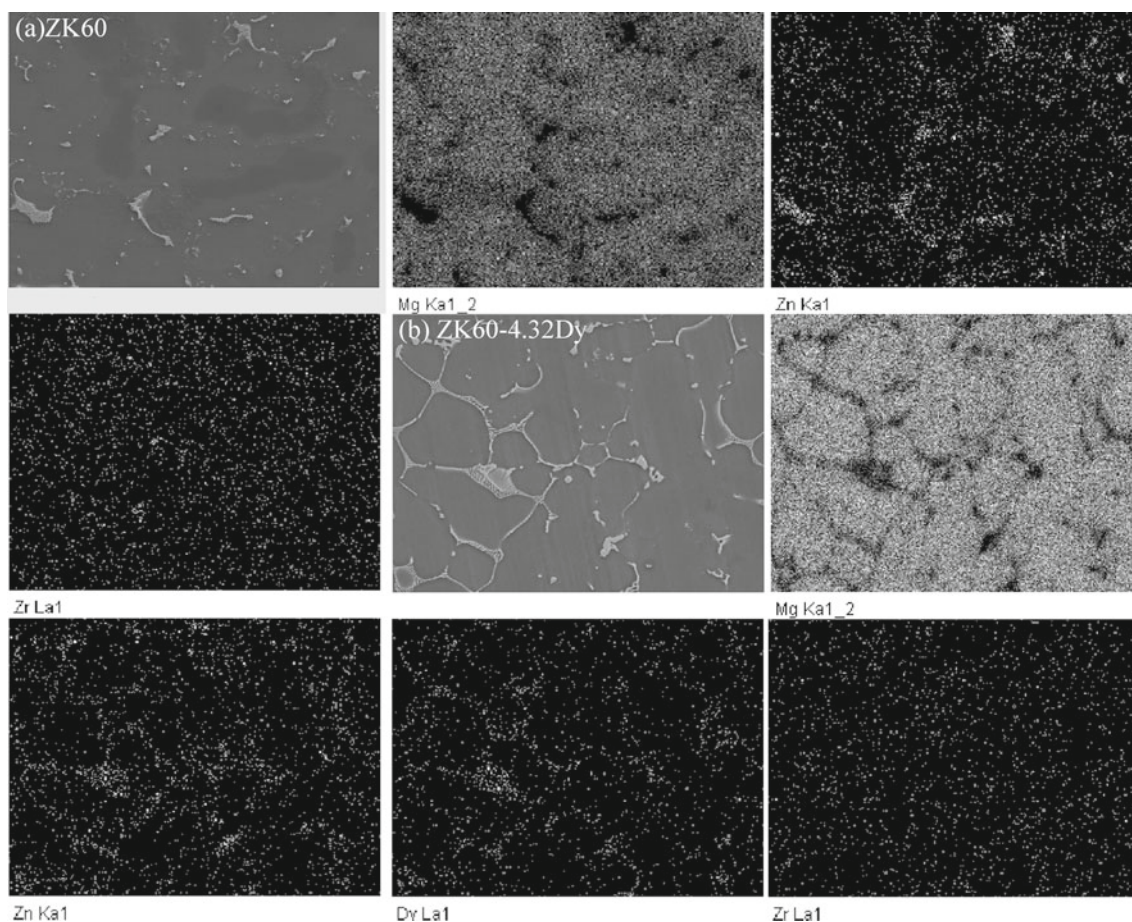


**Figure 5.** Distribution of each element among as-cast microstructures of ZK60– $x$ Dy alloys.

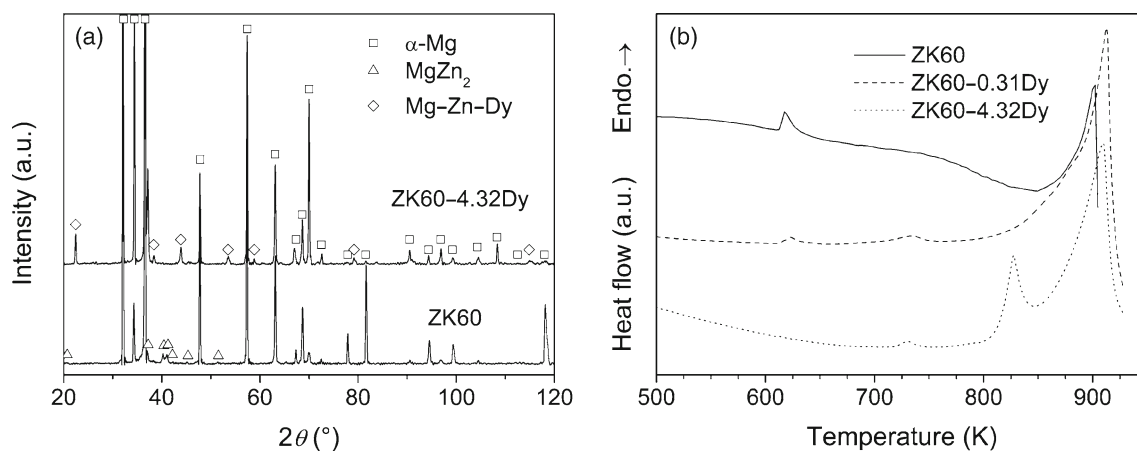


**Figure 6.** XRD spectra (a) and isochronal heating DSC curves (b) of as-cast ZK60– $x$ Dy alloys.

**Table 3.** Peak temperature,  $T_{Pi}$ , of endothermic peaks for isochronal heating of DSC curves of as-cast ZK60– $x$ Dy alloys.

	$T_{P1}$ (K)	$T_{P2}$ (K)	$T_{P3}$ (K)
ZK60	618	902	
ZK60–0.31Dy	622	735	913
ZK60–4.32Dy	731	828	910

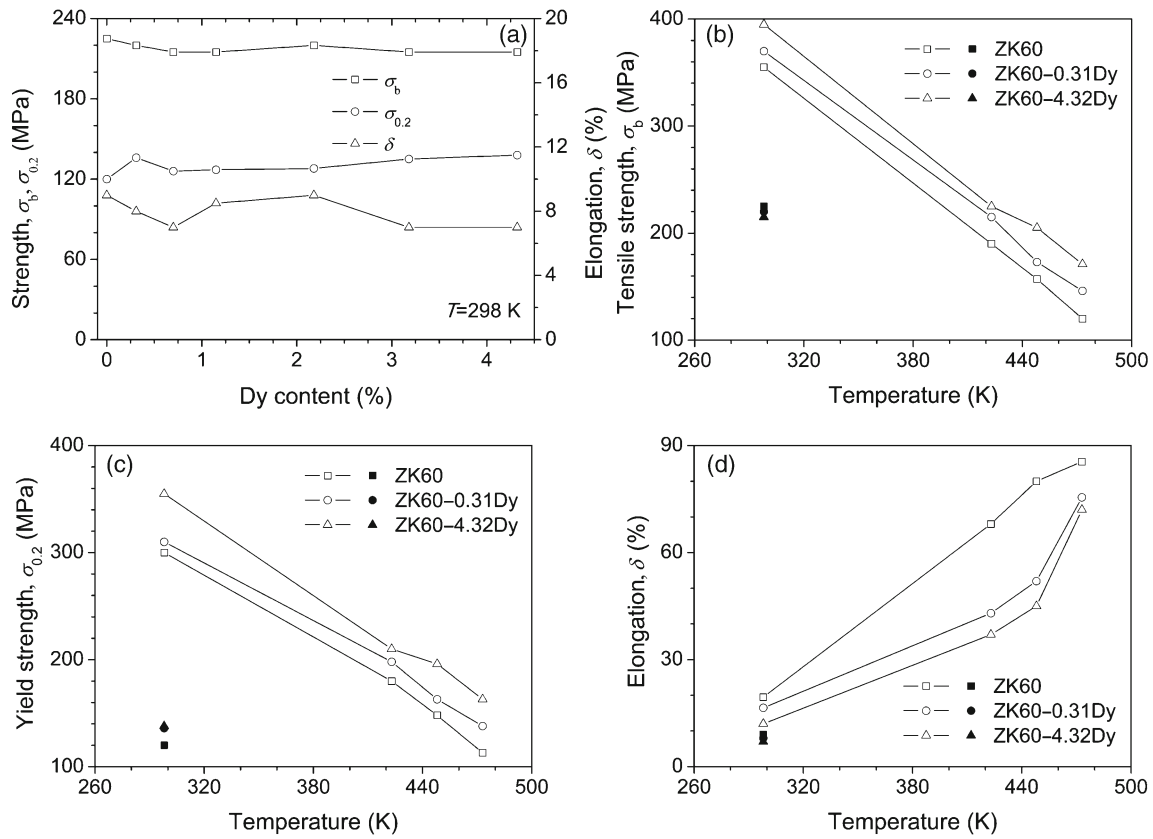


**Figure 7.** Tensile-mechanical properties of as-cast (a) and extruded (b–d) ZK60–xDy alloys. Solid symbols indicate values of as-cast tensile-mechanical properties.

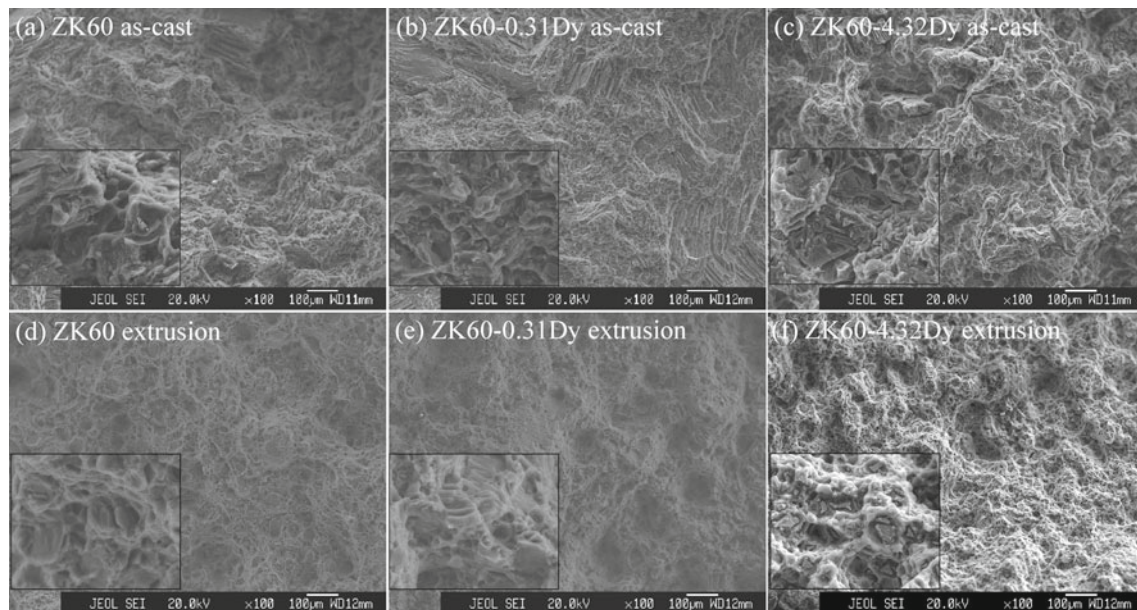


**Figure 8.** SEM morphologies of tensile fractures at ambient temperature of as-cast and extruded ZK60–xDy alloys. Illustrations are local enlarged regions to observe second phase particles at bottom of dimples clearly.

decreases to 157 and 120 MPa at 448 and 473 K, respectively indicating that its application temperature can be considered as 448 K. With increasing Dy content,  $\sigma_b$  and  $\sigma_{0.2}$

increase gradually at each test temperature.  $\sigma_b$  can reach 146 and 171 MPa at 473 K for extruded ZK60–0.31Dy and ZK60–4.32Dy alloys, respectively indicating that the



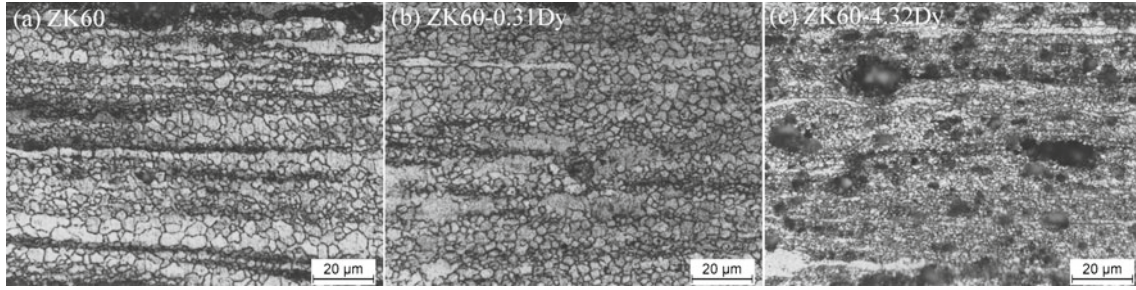


**Figure 9.** Optical graphs in extrusion direction of ZK60–*x*Dy alloys.

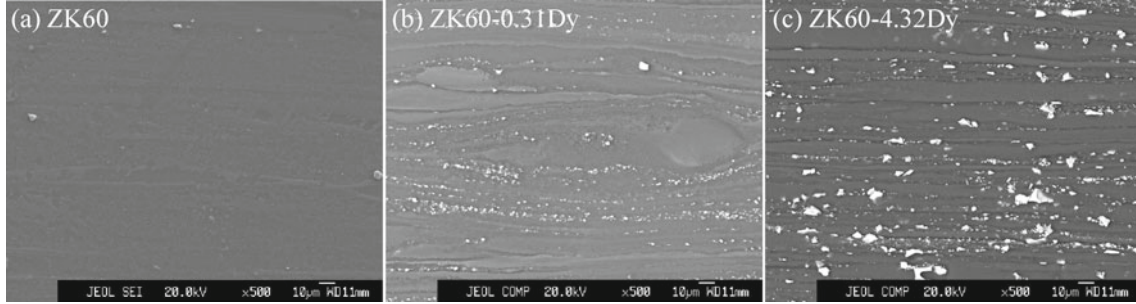


**Figure 10.** SEM graphs in extrusion direction of ZK60–*x*Dy alloys.

application temperature is enhanced to 473 K. However, the increase in the Dy content still reduces the value of  $\delta$  at each test temperature. In summary, the addition of Dy can enhance the tensile mechanical properties of extruded ZK60 alloy at ambient and elevated temperatures. All extruded tensile fractures at ambient temperature exhibit a typical character of ductile fracture (see figure 8d–f). For extruded ZK60 alloy, uniform and deep dimples occupy the majority and meanwhile few fine second phase particles can be observed at the bottom of dimples. With increasing Dy content, dimples become less and shallow and meanwhile second phase particles increase gradually, which is consistent with the gradual decrease in the elongation. Combined with as-cast results, second phase particles at the bottom of dimples should be  $\text{MgZn}_2$  and  $\text{Mg–Zn–Dy}$  phases.

## 4. Discussion

### 4.1 Phase composition

Degree of difficulty in forming compounds between different elements can be judged by electronegativity difference,  $\Delta EN$  and atomic radius difference,  $\Delta r$ . The greater the value of  $\Delta EN$ , the larger the binding force and then easier the formation of compounds. Meanwhile, solid solution with great solubility can be formed when  $\Delta r$  is lower than 15%; otherwise compounds can be formed (Huang *et al* 2004). Electronegativity  $EN$  and atomic radius  $r$  of each element in ZK60–*x*Dy alloys are listed in table 4. On the one hand, Zn–Dy exhibits larger value of  $\Delta EN$  (0.43) than Mg–Zn

**Table 4.** Electronegativity,  $EN$ , atomic radius,  $r$  and growth restriction factor,  $m(k-1)$  of each element in ZK60–*x*Dy alloys (Dean 1999).

	Mg	Zn	Zr	Dy
$EN$	1.31	1.65	1.33	1.22
$r$ (nm)	0.160	0.134	0.160	0.178
$m(k-1)^*$	–	9.93	38.29	4.64

\*Values are calculated when the solute content is the eutectic or peritectic composition, respectively.

and Mg–Dy (0.34 and 0.09, respectively), which leads to greater binding force between Zn and Dy. On the other hand, Zn–Dy exhibits larger value of  $\Delta r$  (33%) than Mg–Zn and Mg–Dy (16 and 11%, respectively), which leads to higher distortion energy and lower structural stability. Therefore, Zn atoms combine with Dy and Mg atoms to form Mg–Zn–Dy new phase on priority.

Distribution of elements Zn and Dy can be explained further by the solidification process. According to the Mg–Zn phase diagram, Mg begins to solidify at 923 K and its eutectic temperature is 614 K where the maximum solubility of Zn is 3 at%. Thus, the temperature interval exceeds 300 K. In addition, elements Zr and Dy with high  $T_m$  can provide the crystalline core easily. Then  $\alpha$ -Mg solid solution can crystallize under a certain undercooling. According to the Mg–Dy phase diagram, the crystallization point of  $\alpha$ -Mg solid solution exceeds 833 K at the Dy content range from 0 to 10 at%,

which cannot reduce its solid-phase point. While, solid solubility of Zn does not exceed 1 at%, when  $\alpha$ -Mg solid solution begins to crystallize above 833 K. Thus, excess Zn atoms still remain within the liquid. As the process carries out, the Zn concentration within the liquid increases gradually and subsequently the solid-phase point decreases gradually. Therefore, Zn atoms plus subsequent Dy atoms are pushed to the grain boundary and then Mg–Zn–Dy phase forms.

#### 4.2 Grain refinement and dynamic recrystallization

Grain refinement mechanism for magnesium alloys is different for different grain-refining methods, however, the basic, starting point is to increase the nucleation rate and inhibit the growth of crystal nuclei. Solute with good segregation and effective nuclei are two essential factors. Solute with good segregation can generate the solutal undercooling at the liquid–solid interface, impede the growth of dendrite and provide the driving force to activate the nucleation. Nucleation capacity of particles determines the start of solidification and number of effective nuclei at the solutal undercooling region. Role of solute element can be expressed by growth restriction factor (GRF) (Chen 2005):

$$\text{GRF} = \sum_i m_i c_{o,i} (k_i - 1), \quad (1)$$

where  $m_i$  is the slope of liquid line of binary phase diagram for the  $i$ th component,  $c_{o,i}$  and  $k_i$  are the original concentration and solute distribution coefficient of the  $i$ th component, respectively. The greater the value of GRF, the stronger the refinement ability. Dy metal exhibits relatively large value of  $m(k-1)$  (see table 4), thus as-cast microstructure is refined effectively.

Refining as-cast microstructure by the addition of Dy can be explained further by the melting point of phase and diffusion rate of atom. Mg–Zn–Dy phase exhibits higher value of  $T_m$  than MgZn<sub>2</sub> phase, which leads to smaller temperature interval,  $\Delta T_m$ , between the former ternary phase and  $\alpha$ -Mg matrix. As the solidification carries on, atoms diffuse on a smaller range to form Mg–Zn–Dy phase. Therefore, as-cast microstructure is refined effectively.

As a softening and grain-refining mechanism for magnesium alloys, dynamic recrystallization can ameliorate the deformation microstructure and enhance the mechanical property effectively (Chen 2005). Among the influencing factors, thermal vibration and atomic diffusion become stronger and nucleation rate for dynamic recrystallization increases as the temperature rises. Low deformation speed is favourable for the nucleation and growth of new grain. Improving the deformation degree can increase the nuclei number of new grains. The finer the original microstructure is, the smaller the DRG is. In addition, second phase particles can hinder the movement of grain boundary undoubtedly (Mao and Zao 1994).

In the present paper, large extrusion ratio ( $\lambda = 40$ ) can generate large deformation degree and ensure adequate

refinement of microstructures and occurrence of dynamic recrystallization. Middle extrusion temperature ( $T = 593$  K) can guarantee not only the occurrence of dynamic recrystallization, but also no easy growth of DRGs. Low extrusion speed ( $V = 1\text{--}2$  m/min) can guarantee fine microstructure. As-cast microstructure is refined gradually with increasing Dy content, thus the corresponding DRGs become smaller gradually. Increasing Mg–Zn–Dy phase with high thermal stability can hinder the growth of DRGs. In addition, the addition of Dy can change the electronic structure of the alloys, increase the bond energy between atoms and enhance the structural stability because Dy atom exhibits more stable external electronic arrangement ( $4f^{10}6s^2$ ) than Mg atom ( $3s^2$ ). Then the formation and movement of large-angle grain boundary are limited and the growth of DRGs is inhibited (Ma *et al* 2003). Therefore, extruded microstructure is refined significantly and  $\bar{d}$  gradually decreases to 1  $\mu\text{m}$  for ZK60–4.32Dy alloy.

#### 4.3 Strengthening mechanism

Grain-refinement strengthening is generally considered as the most important strengthening mechanism for magnesium alloys. Relationship between the yield strength,  $\sigma_y$  and the grain diameter,  $d$  can be expressed by Hall–Petch equation (Hall 1951; Petch 1953):

$$\sigma_y = \sigma_0 + k \cdot d^{-1/2}, \quad (2)$$

where  $\sigma_0$  and  $k$  are the lattice friction force and Petch slope, respectively. Clearly, yield strength increases with decreasing the grain size. Compared with aluminum alloys and steel, magnesium alloys with few independent slip systems exhibit larger value of  $k$  (250–280  $\text{MPa} \cdot \mu\text{m}^{-1/2}$ ). Therefore, grain refinement can improve the strength more effectively.

In the present paper, as-cast microstructure is refined gradually with increasing Dy content. However, second phase also changes significantly in the morphology, distribution and volume fraction, which increases gradually and tends to distribute along grain boundary by continuous network. During the tensile deformation, dislocation piles at the interface between the second phase particles and the  $\alpha$ -Mg matrix, which can lead to stress concentration. When the stress reaches a certain degree, porosities and microcracks initiate. When it exceeds fracture strength, the matrix begins to fracture locally and plasticity decreases significantly. In addition, similar to other second phase such as  $\beta$ -Mg<sub>17</sub>Al<sub>12</sub>, Mg<sub>2</sub>Si, Mg<sub>2</sub>Sn and Al–RE, Mg–Zn–Dy phase should exhibit the incoherent crystal structure with  $\alpha$ -Mg matrix. Taking the two aspects into account, as-cast tensile mechanical property remains almost unchanged.

Extruded microstructure is refined significantly and  $\bar{d}$  decreases gradually to 1  $\mu\text{m}$  for ZK60–4.32Dy alloy, which leads to the prominent strengthening effect by grain refinement. Meanwhile, fine dispersed Mg–Zn–Dy phase can also play a certain role of dispersion strengthening. Therefore,  $\sigma_b$  and  $\sigma_{0.2}$  of extruded alloys are enhanced at ambient



temperature significantly and meanwhile increases gradually with increasing Dy content. In addition, grain refinement is favourable for ameliorating the ductility owing to the following three aspects (Chen 2005): (i) it can shorten the glide path and pile-group length of dislocation, which can make the stress concentration along grain boundary distribute dispersedly and uniformly, (ii) it can make the grain to rotate and the grain boundary move easily and (iii) it can activate other potential non-basal plane slip systems including the prism and pyramidal faces. Among them, activation of the non-basal plane slip system is the most fundamental reason to improve the plasticity significantly for fine-grained magnesium alloys. Therefore, all extruded alloys exhibit larger value of  $\delta$  at ambient temperature. However, second phase among the extruded microstructure still increases gradually with increasing Dy content, which leads to decreasing  $\delta$  to 12% for ZK60–4.32Dy alloy gradually.

DSC analysis indicates that Mg–Zn–Dy phase exhibits higher thermal stability than MgZn<sub>2</sub> phase. For extruded ZK60 alloy, rare MgZn<sub>2</sub> phase plays a weak effect on pinning grain boundary and leads to relatively poor tensile-mechanical property at elevated temperature, where  $\sigma_b$  decreases to 120 MPa at 473 K. With increasing Dy content, Mg–Zn–Dy phase increases gradually and distributes dispersedly. Grain boundary is pinned and its sliding is inhibited effectively at elevated temperature. Therefore, the tensile-mechanical property is enhanced at elevated temperature, where  $\sigma_b$  increases to 171 MPa at 473 K for extruded ZK60–4.32Dy alloy.

## 5. Conclusions

(I) As-cast microstructures of ZK60–*x*Dy alloys mainly consist of  $\alpha$ -Mg matrix, MgZn<sub>2</sub> and Mg–Zn–Dy phases. With increasing Dy content, Mg–Zn–Dy phase increases gradually, while MgZn<sub>2</sub> phase decreases gradually to disappear. Second phase tends to distribute along grain boundary by continuous network. As-cast microstructure is refined gradually, while its tensile-mechanical property remains almost unchanged at ambient temperature.

(II) Extruded microstructure with dispersed second phase is refined obviously and  $\bar{d}$  decreases gradually to 1  $\mu$ m

for ZK60–4.32Dy alloy. Extruded tensile mechanical properties are enhanced at ambient and elevated temperatures.  $\sigma_b$  at 298 and 473 K increases gradually from 355 and 120 MPa for ZK60 alloy to 395 and 171 MPa for ZK60–4.32Dy alloy, respectively. Grain size and second phase play an important role in affecting the tensile-mechanical property of magnesium alloys.

(III) Extruded tensile fractures exhibit a typical character of ductile fracture.

## Acknowledgements

The authors would like to acknowledge the Major Science and Technology Project of Guangdong Province, China (Grant No. 2010A090200078) for financial support.

## References

- Chen Z H 2005 *Wrought magnesium alloys* (Beijing: Chemical Industry Press)
- Dean J A 1999 *Lange's handbook of chemistry* (New York: McGraw-Hill) 15th ed
- Hall E O 1951 *Proc. Phys. Soc.* **B64** 747
- He S M, Peng L M, Zeng X Q, Ding W J and Zhu Y P 2006 *Mater. Sci. Eng.* **A433** 175
- Huang Z H, Guo X F and Zhang Z M 2004 *Trans. Nonferrous Met. Soc. China* **14** 311
- Li D Q, Wang Q D and Ding W J 2011 *Rare Met.* **30** 131
- Li Q, Wang Q D, Wang Y X, Zeng X Q and Ding W J 2007 *J. Alloys Compd.* **427** 115
- Luo Z P, Song D Y and Zhang S Q 1995 *J. Alloys Compd.* **230** 109
- Ma C J, Liu M P and Ding W J 2003 *Mater. Sci. Eng.* **A349** 207
- Mao W M and Zao X B 1994 *The recrystallization and grain growth of metal* (Beijing: Metallurgy Industry Publishing Company)
- Petch N J 1953 *J. Iron Steel Inst.* **174** 25
- Polmear I J 1994 *Mater. Sci. Technol.* **10** 1
- Xia C Q, Wang Y N, Wu A R and Gu Y 2005 *J. Central South Uni. Technol.* **12** 515
- Xu D K, Liu L, Xu Y B and Han E H 2007 *Mater. Sci. Eng.* **A443** 248
- Yu W B, Liu Z Y, He H, Cheng N P and Li X L 2008 *Mater. Sci. Eng.* **A478** 101